Visualization of Localized Holes in Manganite Thin Films with Atomic Resolution

J. X. Ma,[1,2] D. T. Gillaspie,[1,2] E. W. Plummer,[1,2] and J. Shen[1,2,*]

[1]*Condensed Matter Sciences Division, Oak Ridge National Laboratory, Oak Ridge, Tennessee 37831, USA*
[2]*Department of Physics and Astronomy, The University of Tennessee, Knoxville, Tennessee 37996, USA*

(Received 8 July 2005; published 1 December 2005)

The magnetic and transport behaviors of manganites are critically related to the spatial distribution and correlation of doped holes. Using *in situ* scanning tunneling microscopy, we have imaged both occupied and unoccupied states simultaneously in a hole-doped $(La_{5/8-0.3}Pr_{0.3})Ca_{3/8}MnO_3$ epitaxial thin film grown by laser molecular beam epitaxy. Doped holes localized on Mn^{4+} ion sites were directly observed with atomic resolution in the paramagnetic state at room temperature. In contrast to a random distribution, these doped holes show strong short-range correlation and clear preference of forming nanoscale CE-type charge-order-like clusters. The results provide direct visualization of the nature of intriguing electronic inhomogeneity in transition metal oxides.

DOI: 10.1103/PhysRevLett.95.237210 PACS numbers: 75.47.Lx, 71.30.+h, 75.30.Kz, 75.47.Gk

Perovskite manganites are characterized by physical complexity resulting from the coexistence and competition among different kinds of order involving charge, orbital, lattice, and spin degrees of freedom. The strong spin-charge-lattice interaction often leads to fascinating transport properties such as colossal magnetoresistance (CMR) and a rich array of electronic and magnetic phases, which depend sensitively on the hole doping level as well as ionic sizes of elements [1–3]. It has been proposed [4–6] that the polaron effect due to the strong electron-lattice coupling [7] is central to understand the intriguing transport properties of the CMR manganites. Experimentally, research based on scattering studies in reciprocal space has demonstrated that complex polaron effects such as polaron correlation, polaron ordering, and charge localization are critically involved in the metal-insulator transition and intrinsic phase separation [8–16]. However, the formation of small polarons by doped holes is a real-space problem and should be investigated with real-space imaging tools. Thus, the direct observation of doped holes and their correlation is critically needed to understand the microscopic origins of the exotic properties of hole-doped manganites.

As powerful real-space characterization tools, scanning tunneling microscopy (STM) and spectroscopy have been highly successful in studying electronic inhomogeneity and phase separation in layered transition metal oxides (TMOs) [17,18]. However, little has been done for non-layered TMOs, in particular, for the most commonly studied manganites, because they have a 113-perovskite structure which is not cleavable. Although in certain special cases one may have success by cleaning the surfaces of bulk samples [19,20], there is no doubt that epitaxial growth of manganite thin films offers the most reliable and universal means to study the doped holes with atomic resolution using *in situ* STM. In this work, we use epitaxially grown $(La_{5/8-x}Pr_x)Ca_{3/8}MnO_3$ (LPCMO) thin films as a prototype system to study the real-space distribution of the doped holes by means of *in situ* STM in ultrahigh vacuum (base pressure $<1 \times 10^{-10}$ torr). Doped holes localized on Mn^{4+} ion sites were directly observed with atomic resolution in the paramagnetic state at room temperature. In contrast to a random distribution, these doped holes show strong short-range correlation and clear preference of forming nanoscale CE-type charge-order-like clusters. The results provide insights of the nature of the electronic phase separation in the LPCMO compound [21,22], whose driving mechanism is not well understood [23–25].

We grew epitaxial LPCMO thin films on Nb-doped, (001)-oriented $SrTiO_3$ (STO) single crystal substrates by laser molecular beam epitaxy (MBE) (248 nm, 5 Hz, 1 J/cm^2 fluene) under oxygen atmosphere (8% ozone) of about 7 mtorr. STO substrates were chemically etched and *in situ* annealed for 30 minutes at 820 °C before growth [26]. The substrate temperature was kept at 820 °C to allow step-flow growth, which produces a thin film with high quality in terms of minimum oxygen deficiency and other structural defects. After growth, the samples were immediately cooled down to room temperature and transferred to the STM chamber. Samples prepared in this way do not exhibit oxygen deficiency-induced surface reconstruction. All STM images were acquired with mechanically cut Pt-Ir tips at pressure better than 1×10^{-10} torr. A bias voltage is applied to the tip, and the sample is grounded, which means that positive and negative bias images reveal occupied and unoccupied states, respectively. The grown films confirmed all the essential features of ferromagnetic-charge ordering (FM-CO) phase separation, as indicated by the thermal hysteresis behavior in the temperature- and field-dependent magnetization measurements shown in Fig. 1.

Before using STM to identify the doped holes in the LPCMO films, we note that it is well known that the aforementioned surface preparation recipe yields a STO substrate with a Ti-O terminated surface [25]. On such a

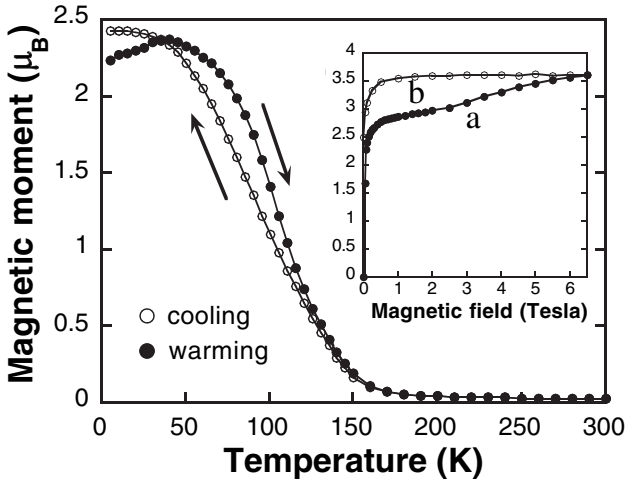

FIG. 1. Temperature dependences of a magnetic moment of LPCMO thin film measured at 0.1 T. Hysteresis is visible in the cooling and warming curves below 160 K due to the coexistence of FM and CO phases. The inset shows the field dependence of magnetic moment measured at 5 K. Curves "a" and "b" represent initial magnetization and subsequent field decreasing. Above 2 T, the CO state starts to transform irreversibly into the FM state and is fully transformed at 6.5 T.

surface, unit cell by unit cell epitaxy of the manganite thin film should lead to a Mn-O terminated surface. Figure 2 shows typical topographic images of a STO substrate and a thin film (120 nm) grown in the step-flow mode. All steps on both the substrate and the films have a height of a single unit cell ($\sim$4 Å), indicating that only one kind of termination layer dominates the surface. Occasionally, we have observed a small area of the surface with another type of termination layer near the step edges (not shown here). Our observation is consistent with previous studies, which confirmed the Mn-O termination in manganite thin films grown on Ti-O terminated STO substrates [27,28].

With the STM operated in the dual bias mode, localized holes in the Mn-O surface layer can be imaged directly

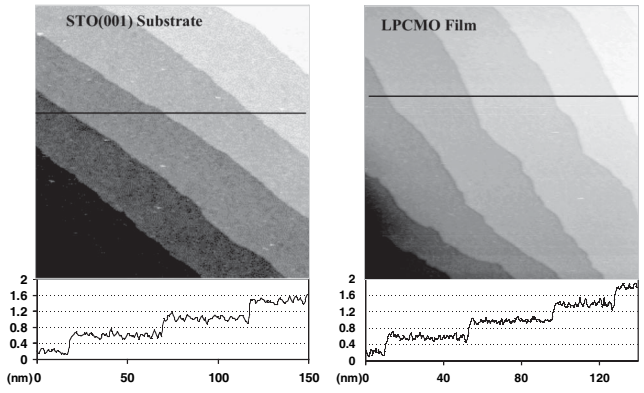

FIG. 2. Typical topographical images of (a) a chemically etched and *in situ* annealed STO (001) substrate and (b) a 120 nm-thick LPCMO thin film. The line profiles show that the steps of both the substrate and the thin film are unit-cell high.

with atomic resolution. Figure 3 shows 20 nm $\times$ 10 nm dual bias STM images obtained simultaneously in the same area at room temperature. A regular square lattice (lattice constant 4 Å) oriented along $\langle 100 \rangle$ directions is clearly visible in both (a) occupied and (b) unoccupied state images. In both images, there are two types of lattice sites with different height contrast. This is best shown in Fig. 3(c) by the marked line profiles taken from the same surface location of the occupied-state (red) and unoccupied-state (black) images. The height difference between the bright and dark sites is particularly large in the unoccupied-state image, which is about 1.0 Å as compared with 0.3 Å in the occupied-state image. Interestingly, the bright sites in the unoccupied-state image become dark sites in the occupied-state image, which is a strong indication that the contrast comes from electronic origin. Recalling the fact that the surface is terminated with a Mn-O plane, it is reasonable to claim that the two types of lattice sites are associated with Mn^{3+} and Mn^{4+} ions. In the unoccupied-state image, the brighter sites should correspond to the locations of the Mn^{4+} ions (localized holes), which have a high-density unoccupied e_g state just above Fermi level that gives rise to a relatively larger tunneling current. The contrast between the Mn^{3+} and the Mn^{4+} sites is reversed and becomes weaker in the occupied-state image, since Mn^{3+} has four (three t_{2g} and one e_g) electrons and Mn^{4+} has three (t_{2g}) electrons below the Fermi level that can contribute to the tunneling current under the experimental bias voltage.

We estimated the ratio between the Mn^{4+} and the Mn^{3+} sites to be about 0.45, which is somewhat lower than the nominal ratio of 0.6 for 3/8 of Ca doping. Intrinsically, there are three likely causes for the reduction of the effective level of hole doping. First, for the Mn-O terminated surface, the hole doping is provided only from below the surface. Second, the e_g electrons are partially localized, which in turn would lead to a reduction of the localized holes in STM images because our STM cannot visualize the dynamic holes. Finally, the polar surface, without being accommodated by surface reconstruction, may be energetically more favorable to adopt a different hole concentration. In addition, the conducting state at the surface could be affected by the broken symmetry effect on the competition between double and superexchange interactions [29,30]. The actual mechanism remains to be investigated further. At this stage, we cannot completely rule out the possibility that there is a variation of Ca concentration near the surface of the LPCMO film, although one would expect an increase of the Mn^{4+} vs Mn^{3+} ratio based on a previous study showing that Ca concentration increased near the surface of a $La_{1-x}Ca_xMnO_3$ thin film [31].

Knowing the spatial distribution of the doped holes at the surface, we now discuss the correlation of the doped holes as compared to a random distribution. We define hole-hole correlation as CO-type and non-CO-type. Those holes occupying neighboring sites along the

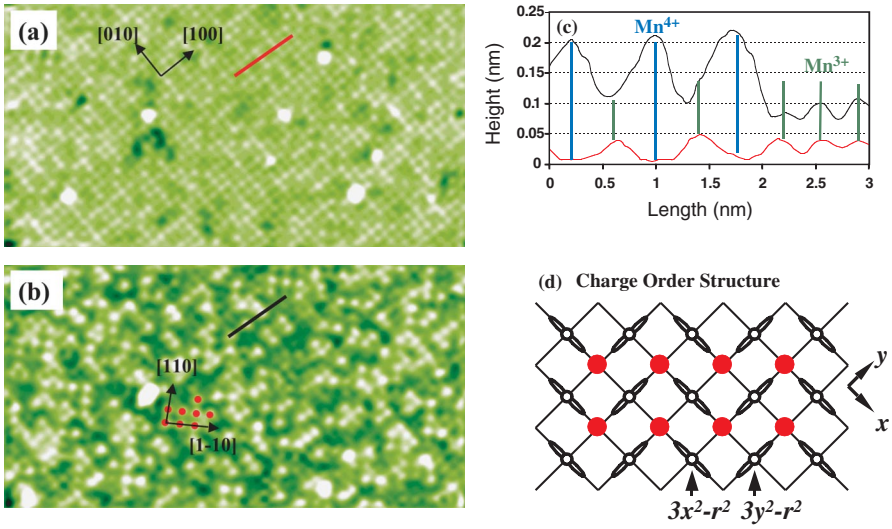

FIG. 3 (color). 20 nm × 10 nm dual bias STM images obtained simultaneously in the same area at paramagnetic state of a 120 nm LPCMO film. (a) Occupied-state image ($V_{bias} = 1.5$ V, $I_t = 0.020$ nA) and (b) unoccupied-state image ($V_{bias} = -2.0$ V, $I_t = 0.050$ nA). Both (a) and (b) reveal the same square lattice of Mn ions. In the unoccupied-state image, the brighter and darker lattice sites correspond to Mn^{4+} (localized hole) and Mn^{3+} ions, respectively. The relative contrast between Mn^{4+} and Mn^{3+} ions is reversed in the occupied-state image. (c) Marked line profiles showing the relative contrast between Mn^{4+} (indicated by blue lines) and Mn^{3+} (indicated by green lines) ions. The CE-type CO cluster is indicated by the red spots in the unoccupied-state image, with a schematic picture shown in (d).

[110] and/or [1$\bar{1}$0] directions are viewed as CE-type CO clusters as indicated (red dots) in Fig. 3(b) and shown schematically in Fig. 3(d). Neighboring holes along the [100] and/or [010] directions are viewed as non-CO clusters. Figure 4 shows the statistical distribution of the non-CO and CO clusters obtained from Fig. 3(b), which is compared with that of a two-dimensional random distribution (2DRD) with the same doping level [32]. The distribution of localized holes in Fig. 3(b) is distinctively different from that of the 2DRD. In particular, the experimental data show a strong preference of forming small sized non-CO clusters. The average size of the non-CO cluster sizes obtained from Fig. 3(b) is 1.9 holes, which is considerably smaller than that of the 2DRD (2.6 holes). This observation indicates a strong short-range hole-hole correlation, and the formation of larger clusters is energetically unfavorable in the paramagnetic state. Moreover, the number of the CE-like CO clusters obtained from the STM data is distinctly higher than that of the random distribution. These differences, however, should reflect only the behavior of static doped holes, since our STM is not sensitive to the dynamic motion of the holes. Our result demonstrated that, for LPCMO, CO clusters are preserved even in the paramagnetic state at a temperature that is well above the CO transition temperature, which is consistent with previous x-ray scattering studies of manganites [13,15]. An important and open question is whether the hole localization and the electronic inhomogeneity in the LPCMO film is spatially correlated to the doped divalent cations (Ca). This issue will be addressed in future studies by controlling the termination layer of the film.

Our results demonstrate that the combination of laser MBE growth and *in situ* STM with atomic resolution is a powerful approach to study TMOs. Direct visualization of the doped holes in real space provides insights of polaron

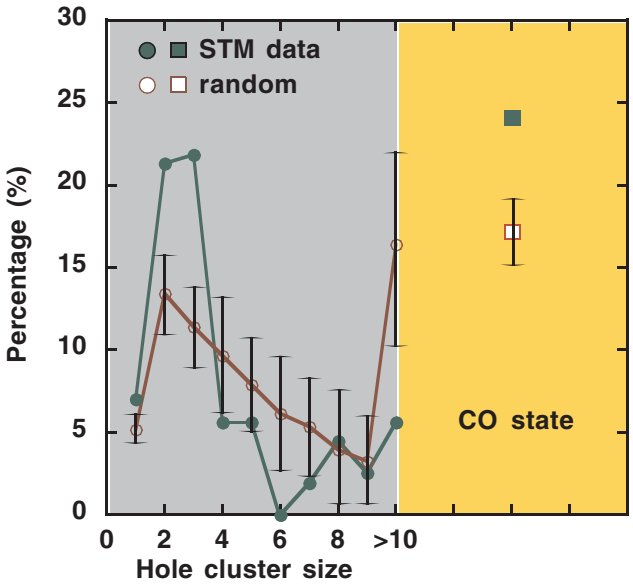

FIG. 4 (color). Distribution of holes forming the non-CO (left panel) and CO (right panel) clusters (normalized by total number of holes) obtained from Fig. 3(b), which is compared with that of a 2DRD with the same doping level. The error bars represent the standard deviations for the random distribution when using the same number of holes from the experimental data. In comparison to the random distribution, the localized holes show strong short-range correlation and a clear preference of forming nanoscale CE-type charge-order-like clusters.

correlation in the manganite films. This work will stimulate further experiments on other manganite materials so that a comprehensive understanding of electronic inhomogeneity in hole-doped manganites at the atomic scale can be reached.

We are grateful to E. Dagotto, T. Egami, and P. Dai for valuable discussions. Oak Ridge National Laboratory (ORNL) is managed by UT-Battelle, LLC for the U.S. Department of Energy under Contract No. DE-AC05-00OR22725.

*Corresponding author.
Electronic address: shenj@ornl.gov

[1] M. Imada, A. Fujimori, and Y. Tokura, Rev. Mod. Phys. **70**, 1039 (1998).
[2] E. Dagotto, T. Hotta, and A. Moreo, Phys. Rep. **344**, 1 (2001).
[3] M. B. Salamon and M. Jaime, Rev. Mod. Phys. **73**, 583 (2001).
[4] A. J. Millis, P. B. Littlewood, and B. I. Shraiman, Phys. Rev. Lett. **74**, 5144 (1995).
[5] H. Roder, J. Zang, and A. R. Bishop, Phys. Rev. Lett. **76**, 1356 (1996).
[6] T. Egami and D. Louca, Phys. Rev. B **65**, 094422 (2002).
[7] G. M. Zhao, K. Conder, H. Keller, and K. A. Muller, Nature (London) **381**, 676 (1996).
[8] V. Kiryukhin, New J. Phys. **6**, 155 (2004).
[9] J. M. de Teresa *et al.*, Nature (London) **386**, 256 (1997).
[10] Y. Yamada *et al.*, Phys. Rev. Lett. **77**, 904 (1996).
[11] P. Dai *et al.*, Phys. Rev. Lett. **85**, 2553 (2000).
[12] A. Lanzara, N. L. Saini, M. Brunelli, F. Natali, and A. Bianconi, Phys. Rev. Lett. **81**, 878 (1998).
[13] C. S. Nelson *et al.*, Phys. Rev. B **64**, 174405 (2001).
[14] S. J. L. Billinge, Th. Proffen, V. Petkov, J. L. Sarro, and S. Kycia, Phys. Rev. B **62**, 1203 (2000).
[15] K. H. Kim, M. Uehara, and S.-W. Cheong, Phys. Rev. B **62**, R11 945 (2000).
[16] V. Kiryukhin *et al.*, Phys. Rev. B **65**, 094421 (2002).
[17] M. Vershinin *et al.*, Science **303**, 1995 (2004).
[18] S. H. Pan *et al.*, Nature (London) **413**, 282 (2001).
[19] M. Fäth *et al.*, Science **285**, 1540 (1999).
[20] Ch. Renner, G. Aeppli, B.-G. Kim, Yeong-Ah Soh, and S.-W. Cheong, Nature (London) **416**, 518 (2002).
[21] M. Uehara, S. Mori, C. H. Chen and S.-W. Cheong, Nature (London) **399**, 560 (1999).
[22] L. Zhang, C. Israel, A. Biswas, R. L. Greene, and A. D. Lozanne, Science **298**, 805 (2002).
[23] A. Moreo, M. Mayr, A. Feiguin, S. Yunoki, and E. Dagotto, Phys. Rev. Lett. **84**, 5568 (2000).
[24] P. G. Radaelli *et al.*, Phys. Rev. B **63**, 172419 (2001).
[25] K. H. Ahn *et al.*, Nature (London) **428**, 401 (2004).
[26] M. Kawasaki *et al.*, Science **266**, 1540 (1994).
[27] H. Kumigashira *et al.*, Appl. Phys. Lett. **82**, 3430 (2003).
[28] P. R. Broussard, S. B. Qadri, V. M. Browning, and V. C. Castone, Appl. Surf. Sci. **115**, 80 (1997).
[29] H. Zenia, G. A. Gehring, G. Banach, and W. M. Temmerman, Phys. Rev. B **71**, 024416 (2005).
[30] A. Filippetti and W. E. Pickett, Phys. Rev. B **62**, 11 571 (2000).
[31] J. Choi, J. Zhang, S.-H. Liou, P. A. Dowben, and E. W. Plummer, Phys. Rev. B **59**, 13 453 (1999).
[32] The 2DRD model includes two steps to generate the 2DRD data in Fig. 4: (1) We generated randomly distributed holes on 500×500 sites and obtained the size distribution as a standard 2DRD distribution denoted as $N_{i,s}$, with i being the size of the hole clusters; (2) we generate 20 sets of randomly distributed holes on the same lattice sites as Fig. 3 and then used the size distribution for each set ($N_{i,j}$) to calculate the standard deviation with respect to $N_{i,s}$.